MULTIAXIAL CYCLIC THERMOPLASTICITY ANALYSIS WITH BESSELING'S SUBVOLUME METHOD

R. L. McKnight
General Electric Co.
Cincinnati, Ohio 45215

Abstract

In 1975, a modification was formulated to Besseling's Subvolume Method to allow it to use multilinear stress-strain curves which are temperature dependent to perform cyclic thermoplasticity analyses. This method automotically reproduces certain aspects of real material behavior important in the analysis of Aircraft Gas Turbine Engine (AGTE) components. These include the Bauschinger effect, cross-hardening, and memory. This constitutive equation has been implemented in a finite element computer program called CYANIDE which has been in production usage since 1977. Subsequently, classical time dependent plasticity (creep) was added to the program. Since its inception, this program has been assessed against laboratory and component testing and engine experience. The ability of this program to simulate AGTE material response characteristics has been verified by this experience and its utility in providing data for life analyses has been demonstrated. In this area of life analysis, the multiaxial thermoplasticity capabilities of the method have proved a match for the actual AGTE life experience. This paper will explore the multiaxial, variable-temperature nature of the method and show examples demonstrating its utility.

BESSELING'S MATHEMATICAL MODEL

The relation between the deviatoric stresses and the deviatoric strains is given by

$$S_{ij} = 2G(e_{ij} - e''_{ij}) \tag{1}$$

where

S_{ij} is the deviatoric stress tensor

e_{ij} is the total deviatoric strain tensor

e''_{ij} is the plastic strain tensor

G is the shear modulus

The yield strain, P, is given by the plastic potential function

$$g = (e_{ij} - e''_{ij})(e_{ij} - e''_{ij}) - P^2 = 0 \tag{2}$$

The incremental plastic strains are given by

$$\delta e''_{ij} = \frac{(e_{ij} - e''_{ij})(e_{hk} - e''_{hk})}{P^2} \delta e_{hk} \tag{3}$$

provided that

$$(e_{hk} - e''_{hk})\delta e_{hk} > 0 \tag{4}$$

The incremental stress-strain relation is

$$\delta S_{ij} = 2G\left[\delta e_{ij} - \frac{(e_{ij} - e''_{ij})(e_{hk} - e''_{hk})}{p^2}\,\delta e_{hk}\right. \tag{5}$$

The new vield strain, $e_{ij} + \delta e_{ij}$, is determined from

$$\delta g = 2(e_{ij} - e''_{ij})(\delta e_{ij} - \delta e''_{ij}) = 0 \tag{6}$$

Besseling then introduced the concept of elastic-perfectly plastic subvolumes. The elastic potential, ϕ_1, of the subvolume of density ρ after prior plastic flow is given by

$$\rho\,\phi_1 = G(e_{ij} - \bar{e}_{ij1})(e_{ij} - \bar{e}_{ij1}) \tag{7}$$

where the $\bar{e}_{ij1}$ are the plastic strains due to ideal plastic yielding. If this subvolume constitutes the fraction ψ of the volume element dV, its contribution to the total elastic potential of dV is

$$\psi G(e_{ij} - \bar{e}_{ij1})(e_{ij} - \bar{e}_{ij1})dV \tag{8}$$

If k subvolumes of the volume dV have exceeded their critical value of elastic potential and undergone plastic flow, the total elastic potential is given by

$$\rho\phi dV = \left[Ge_{ij}e_{ij}\left(1 - \sum_1^k \psi_n\right) + G\sum_1^k \psi_n(e_{ij} - \bar{e}_{ijn})(e_{ij} - \bar{e}_{ijn})\right]dV \tag{9}$$

Now, the deviatoric stress tensor is given by

$$S_{ij} = 2G\left[\left(1 - \sum_1^k \psi_n\right)e_{ij} + \sum_1^k \psi_n(e_{ij} - \bar{e}_{ijn})\right] \tag{10}$$

After yielding, the elasticity limit of subvolume k is given by

$$g_k = (e_{ij} - \bar{e}_{ijk})(e_{ij} - \bar{e}_{ijk}) - P_k^2 = 0 \tag{11}$$

The subvolume incremental plastic strains are given by

$$\delta\bar{e}_{ijk} = \frac{(e_{ij} - \bar{e}_{ijk})(e_{\alpha\beta} - \bar{e}_{\alpha\beta k})}{P_k^2} \delta e_{\alpha\beta k} \tag{12}$$

provided that

$$(e_{\alpha\beta k} - \bar{e}_{\alpha\beta k})\delta e_{\alpha\beta k} > 0 \tag{13}$$

The incremental stress-strain relations are

$$\delta S_{ij} = 2G\left[\delta e_{ij} - \sum_1^k \psi_n \frac{(e_{ij} - \bar{e}_{ijn})(e_{\alpha\beta} - \bar{e}_{\alpha\beta n})}{P_n^2} \delta e_{\alpha\beta}\right] \tag{14}$$

DEVELOPMENT OF NONISOTHERMAL CAPABILITY

The equation relating the stresses and the subvolume strains, Equation (10), can be rewritten to give

$$S_{ij} = 2G[e_{ij} - \Sigma\psi_n \bar{e}_{ijn}] \tag{15}$$

Now these stresses must be the same as the stresses given by Equation (1). Therefore, the two right-hand sides can be equated. When this is done, we get

$$\sum_{1}^{k} \psi_n \bar{e}_{ijn} = e''_{ij} \tag{16}$$

which gives a relationship between the subvolume plastic strains and the total plastic strains.

Squaring both sides of Equation (16) and multiplying by 2/3, we get

$$\frac{2}{3}\left(\sum_{1}^{k} \psi_n\right)^2 \bar{e}_{ijn}\, \bar{e}_{ijn} = \frac{2}{3}\, e''_{ij}\, e''_{ij} \tag{17}$$

Now

$$\varepsilon_p = \sqrt{\frac{2}{3}\, e''_{ij}\, e''_{ij}} \tag{18}$$

Therefore

$$\varepsilon_p = \psi_1 \varepsilon_{p1} + \psi_2 \varepsilon_{p2} + \psi_3 \varepsilon_{p3} + \ldots + \psi_n \varepsilon_{pn} \tag{19}$$

This gives a relationship between the total effective plastic strain and the subvolume effective plastic strains.

The following ratio can be formed between a subvolume effective plastic strain and the total effective plastic strain:

$$\left(\frac{\varepsilon_{pn}}{\varepsilon_p}\right)^2 = \frac{\frac{2}{3}\, \bar{e}_{ijn}\, \bar{e}_{ijn}}{\frac{2}{3}\, e''_{ij}\, e''_{ij}} \tag{20}$$

or

$$\bar{e}_{ijn}\, \bar{e}_{ijn} = \left(\frac{\varepsilon_{pn}}{\varepsilon_p}\right)^2 e''_{ij}\, e''_{ij} \tag{21}$$

By taking the square root of both sides, we obtain

$$\bar{e}_{ijn} = \frac{\varepsilon_{pn}}{\varepsilon_p} e''_{ij} \tag{22}$$

This gives a means of determining the subvolume plastic strains from the total plastic strains if the effective plastic strains are known.

This then provides the tools to convert Besseling's isothermal theory into a nonisothermal theory. We note that for variable temperature problems g and g_k will be functions of both strain and temperature.

$$g = g\ (e_{ij}, T) \tag{23}$$

$$g_k = g_k(e_{ij}, T) \tag{24}$$

These functions can be specified by defining temperature dependent stress-strain curves.

For incremental loading including temperature changes, the change in the plastic potential function is given by

$$dg = \frac{\partial g}{\partial e_{ij}} de_{ij} + \frac{\partial g}{\partial T}\ dT \tag{25}$$

There are three possible conditions that can occur due to this load increment and these are determined by the value of this differential.

For loading beyond the present yield surface

$$dg > 0 \tag{26}$$

$$\frac{\partial g}{\partial e_{ij}} de_{ij} + \frac{\partial g}{\partial T} dT > 0 \tag{27}$$

For the loading to place the point on the new yield surface

$$dg = 0 \tag{28}$$

$$\frac{\partial g}{\partial e_{ij}} de_{ij} + \frac{\partial g}{\partial T} dT = 0 \tag{29}$$

For the point to unload back into the elastic range

$$dg < 0 \tag{30}$$

$$\frac{\partial g}{\partial e_{ij}} de_{ij} + \frac{\partial g}{\partial T} dT < 0 \tag{31}$$

These last two conditions are used to accomodate temperature variations. The solution to any load condition, (N-1), is arrived at when

$$dg_{n-1} = \frac{\partial g}{\partial e_{ij}} de_{ij/T = \text{Constant}} \leq 0 \tag{32}$$

In proceeding to the next load step, (N), the temperature effects on the stress-strain curve are incorporated so as not to vialate this condition while holding the strains constant.

$$dg_{(n-1),(N)} = \frac{\partial g}{\partial T} dT = 0 \tag{33}$$

Thus, we are requiring that the change of temperature alone not effect the inelastic condition of the material. We accomplish this by realizing that

$$\frac{\partial g}{\partial T} dT = - \frac{2G}{\lambda} de^{e}_{ij} de^{p}_{ij} \tag{34}$$

Therefore, by requiring that

$$de^{p}_{ij} = 0 \tag{35}$$

We force

$$\frac{\partial g}{\partial T} dT = 0 \tag{36}$$

This then gives us the mechanism for positioning our new yield surfaces in step, N. The step, N, solution then proceeds by applying the loads and boundary conditions and iterating to obtain

$$dg = \frac{\partial g}{e_{ij}} de_{ij} \leq 0 \tag{37}$$

within your specified convergence tolerance.

CREEP ANALYSIS

The creep analysis utilizes one of two possible creep representations. When tertiary creep is not considered to be of importance, the equation used is

$$\epsilon_c = k\bar{\sigma}_e^n t^m + q\bar{\sigma}_e^r t \tag{38}$$

where

$\bar{\sigma}_e = \sigma_e/100000$, σ_e = effective stress

k, m, n, q, r = material-dependent and temperature-dependent creep coefficients.

When the material exhibits a significant amount of tertiary creep capability, an alternate representation is used. Primary creep is represented by the Bailey-Norton law.

$$\epsilon_c^P = A_1 \bar{\sigma}_e^{A_2} t^{A_3} \tag{39}$$

Secondary creep is modeled with the expression proposed by Marin, Pao, and Cuff (Reference 19)

$$\epsilon_c^S = A_4\bar{\sigma}_e^{A_5} t + A_6 \bar{\sigma}_e^{A_7} \tag{40}$$

Tertiary creep is represented with an equation of the form

$$\epsilon_c^T = A_8 e^{A_9} \bar{\sigma}_e^{A_{10} t} \tag{41}$$

$A_1, A_2, \ldots A_{10}$ = material-dependent and temperature dependent creep coefficients.

CYANIDE also contains an orthotropic creep formulation. The creep strain rate is assumed to be given by

$$\dot{\epsilon}_{ij} = g_{ijkl}\sigma_{kl} \tag{42}$$

where

$\dot{\epsilon}_{ij}$ = strain rate tensor

σ_{kl} = stress tensor

g_{ijkl} = Tensor whose components are functions of temperature, σ_e, and hardening rule and are derivable from input creep curves.

The user can select from time hardening, strain hardening, or life fraction creep rule, depending upon the actual material characteristics. Strain hardening is ordinarily adequate for describing hardening behavior, providing that stress reversals do not occur. A stress reversal is considered to occur when

$$\epsilon_{ij}^c \dot{\sigma}_{ij} < 0 \tag{43}$$

Where ϵ_{ij}^c is creep strain measured from its current origin. When a reversal occurs, the origin is changed and the analysis proceeds (Reference 20) .

The combination of general creep equations and creep rule makes the program very general in its application to structures which undergo time-dependent plastic flow in which transient effects are not significant.

CYANIDE COMPUTER PROGRAM

Many of the steps in the CYANIDE nonlinear finite element computer program are the same as those for a linear finite element analysis. The nonlinear effects are introduced into the system of finite element equations by adding vectors of pseudoforces to the right hand side.

$$|K| \{\delta\} = \{F\} + \{F_p\} + \{F_c\} \tag{44}$$

where

$|K|$ is the elastic stiffness matrix.

$\{\delta\}$ is the vector of nodal displacements.

$\{F\}$ is the force vector including thermal terms.

$\{F_p\}$ is the plastic pseudoforce vector.

$\{F_c\}$ is the creep pseudoforce vector.

For each increment of loading, the nonlinear pseudoforces are iterated upon until the requirements of equilibrium, compatability, and the constitutive equations are met within user specified tolerances. Since this method does not require modification of the stiffness matrix during iterations it is very economical. This economy is magnified during cyclic analysis. The stiffness matrix need only be regenerated if the material properties are revised by thermal variation or if elements have been added or removed.

MULTIAXIAL, VARIABLE TEMPERATURE EXAMPLE

In a previous NASA contract, we investigated one of the common thermal stress problems in AGTE's: turbine blade tip cracking. In that case, the critical region was shown by analysis and confirmatory testing to have the cyclic stress-strain behavior noted in Figure 1. High temperature, time dependent flow rapidly relaxes the compressive stress such that on cool-down high tensile stresses are genrated. This process shakes down very rapidly to an almost elastic hysteresis loop based on modulus changes. In that case the problem was almost totally uniaxial in nature.

A second type of thermal stress problem prevalent in AGTE's is the hot spot. In this case, the stress strain response is definitely multiaxial. We will investigate a hot spot on a combustor shingle as being typical of these problems. Figure 2 shows a shingle segment. Taking advantage of its large radius of curvature and thinness, it was modeled as a flat plate in a condition of plane stress. The model is shown in Figure 3. Figures 4, 5 and 6 show the nature of the hot spot at peak temperature and Figure 7 shows the heat-up cool-down temperature cycle at the center of the hot spot. This cycle was analyzed assuming no time dependent effects occcurred during heat-up and cool-down but that a one hour hold time was associated with the peak of the hot spot.

The stress-strain results of the first cycle are shown in Figures 8, 9 and 10 for the center of the hot spot. Figure 8 shows effective stress versus effective strain and Figures 9 and 10 show the biaxial stresses versus strains. Once again the effect of plasticity and creep is to generate tensile stresses during the cool-down portion of the cycle. The next series of figures shows the shakedown stress-strain results for the center of the hot spot. Figure 11 shows the effective stress versus effective strain shakedown values and Figures 12 and 13 show the shakedown biaxial stress cycle at the center of the hot spot. Thus this multiaxial thermal stress case, just as the uniaxial case, shakes down to almost elastic cycling with a high tensile mean stress. In addition, the stresses are almost proportional. These types of analyses are important in indicating the types of response and life tests needed.

REFERENCES

1. Besseling, J. F., "A Theory of Plastic Flow for Anisotropic Hardening in Plastic Deformation of an Initially Isotropic Material", Report S.410, National Aeronautical Research Institute, Amsterdam, 1953.
2. Besseling, J. F., "A Theory of Elastic, Plastic, and Creep Deformations of an Initially Isotropic Material", SUDAER No. 78, Stanford University, April, 1958.
3. Besseling, J. F., "A Theory of Elastic, Plastic, and Creep Deformations of an Initially Isotropic Material Showing Anisotropic Strain-Hardening, Creep Recovery, and Secondary Creep", J. of Applied Mechanics, pp. 529-536, December, 1958.
4. Duwez, P., "On the Plasticity of Crystals", Physical Review, Vol. 47, p. 494, 1935.
5. White, G. N., Jr., "Application of the Theory of Perfectly Plastic Solids to Stress Analysis of Strain Hardening Solids", Graduate Division of Applied Mathematics, Brown University, Tech. Rpt. 51, 1950.
6. Turner, J. J., Clough, R. W., Martin, H. C., and Topp, L. J., "Stiffness and Deflection Analysis of Complex Structures, Journal of the Aeronautical Sciences, Vol. 23, No. 9, p. 805, Sept., 1956.
7. Armen, H. Jr., "Plastic Analysis", Structural Mechanics Computer Programs, edited by Pilkey, W., Saczalski, K., and Schaeffer, H., University Press of Virginia, 1974, pp. 37-79.
8. Armen, H., Jr., Pifko, A., and Levine, H. S., "Finite Element Analysis of Structures in the Plastic Range", NASA CR-1649, February, 1971.
9. Armen, H., Jr., Levine, H. S., and Pifko, A. B., "Plasticity - Theory and Finite Element Applications", Proc. of 2nd U.S.-Japan Seminar on Matrix Methods of Structural Analysis and Design, pp. 393-437, August 1972.
10. Witmer, E. A., Kotanchik, J. J., "Progress Report on Discrete-Element Elastic and Elastic-Plastic Analyses of Shells of Revolution Subjected to Axisymmetric and Asymmetric Loading", Proc. of the Second Conference on Matrix Methods in Structural Mechanics, WPAFB, pp. 1341-1453, December, 1969.
11. Wilson, E. L., "Finite Element Analysis of Two-Dimensional Structures", University of California, Structures and Materials Research Department of Civil Engineering, Report No. 63-2, June, 1963.
12. Salmon, M., Berke, L., and Sandhu, R., "An Application of the Finite Element Method to Elastic-Plastic Problems of Plane Stress", Air Force Flight Dynamics Laboratory, Tech. Rpt. AFFDL-TR-68-39, May, 1970.
13. Zienkiewicz, D. C., The Finite Element Method in Engineering Science, McGraw-Hill, New York, 1971.
14. Marin, J., Ulrich, B. H., and Hughes, W. P., "Plastic Stress-Strain Relations for 75S-T6 Aluminum Alloy Subjected to Biaxial Tensile Stresses", NACA TN2425, National Advisory Committee for Aeronautics, Washington, D.C., August, 1951.
15. Ueda, Y., and Yamakawa, T., "Thermal Stress Analysis of Metals with Temperature Dependent Mechanical Properties", Mechanical Behavior of Materials Vol. 3, edited by Taira, S., and Kunugi, M., The Society of Materials Science, Japan, pp. 10-20, 1972.
16. Hunsaker, B., Jr., Vaughn, D. K., Stricklin, J. A., and Haisler, W. E., "A Comparison of Current Work Hardening Models Used in the Analysis of Plastic Deformations", Texas A&M University, Texas Engineering Experiment Station, TEES-RPT-2926-73-3, October, 1973.

17. McKnight, R. L., "Finite Element Cyclic Thermoplasticity Analysis by the Method of Subvolumes", Ph.D. dissertation, University of Cincinnati, 1975.
18. McKnight, R. L. and Sobel, L. H., "Finite Element Cyclic Thermoplasticity Analysis by the Method of Subvolumes," Comput. Structures, Vol. 7, No. 3, 1977.
19. Marin, J., Pao, Y. H., and Cuff, G., "Creep Properties of Lucite and Plexiglass for Tension, Compression, Bending, and Torsion," Trans. ASME 73, 705, 1951.
20. Pugh, C. E., "Constitutive Equations for Creep Analysis of Liquid Moderated Fast Breeder Reactor (LMFBR) Components," in Advances in Design for Elevated Temperature Environment, S. Y. Zamrik and N. I. Jetter, Eds. ASME, 1975.

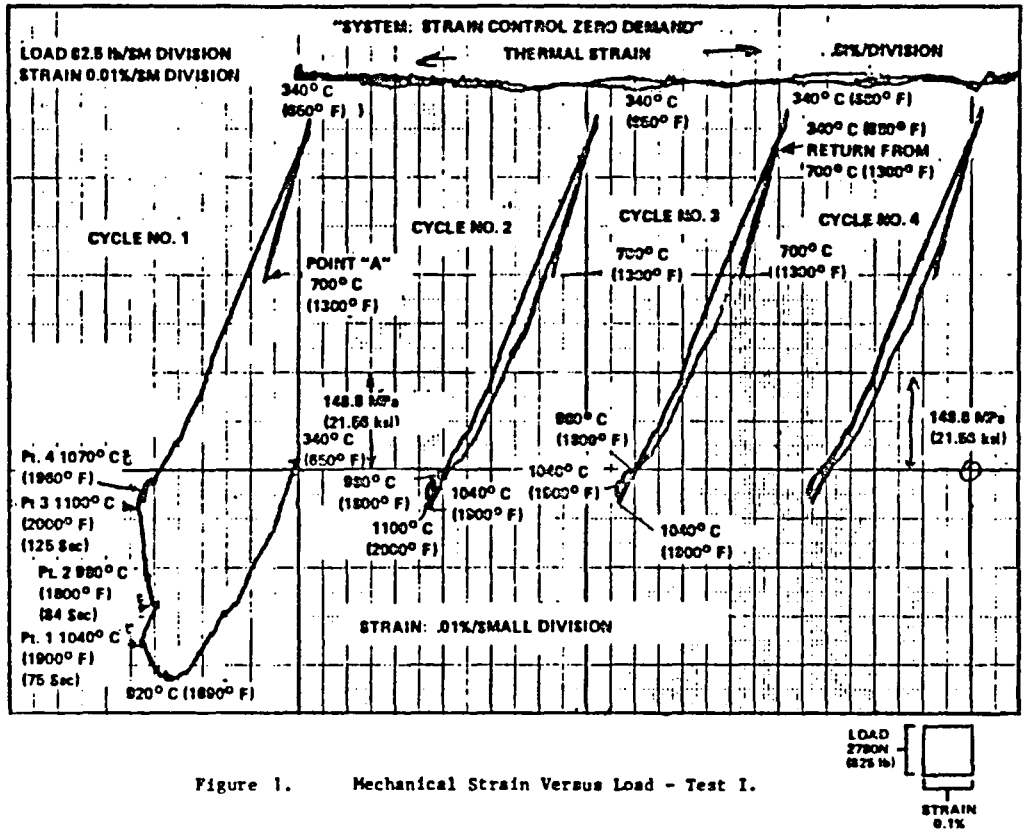

Figure 1. Mechanical Strain Versus Load - Test I.

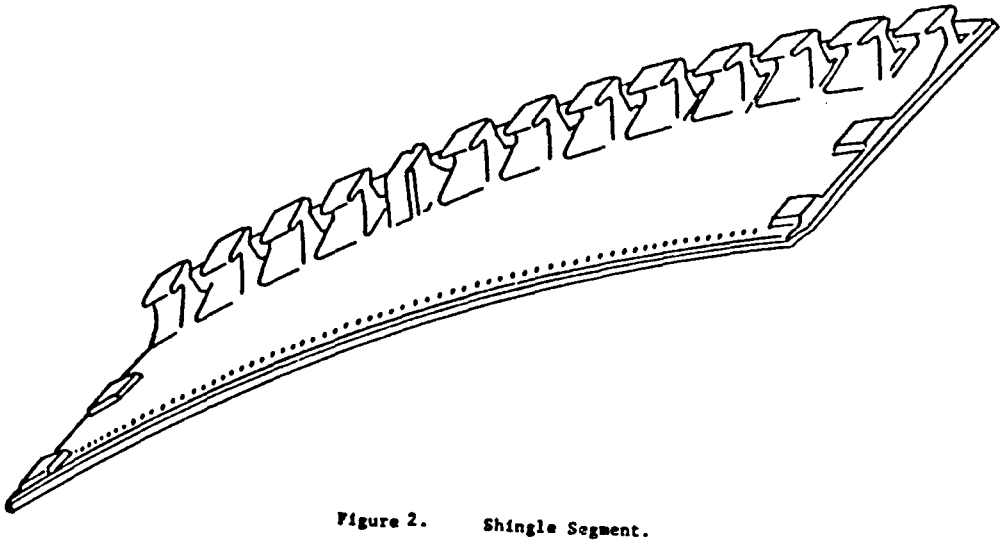

Figure 2. Shingle Segment.

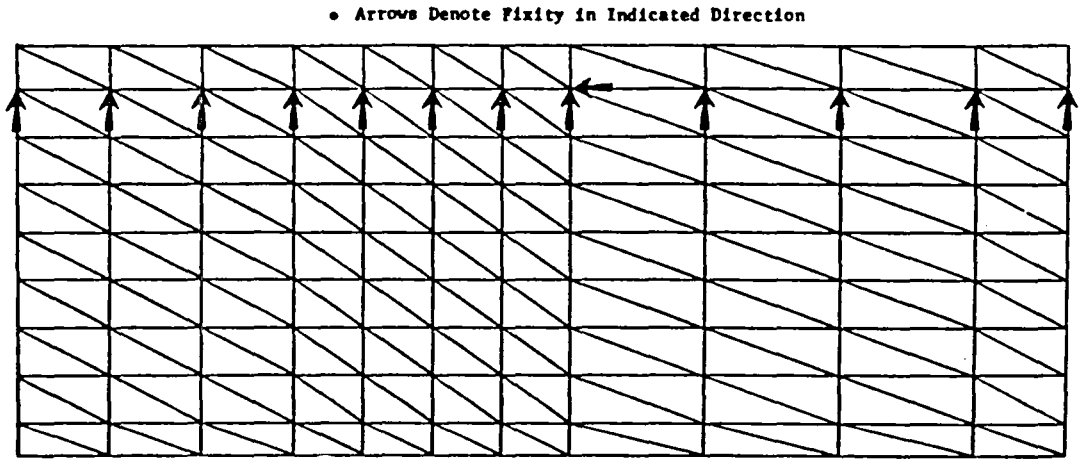

Figure 3. Boundary Conditions.

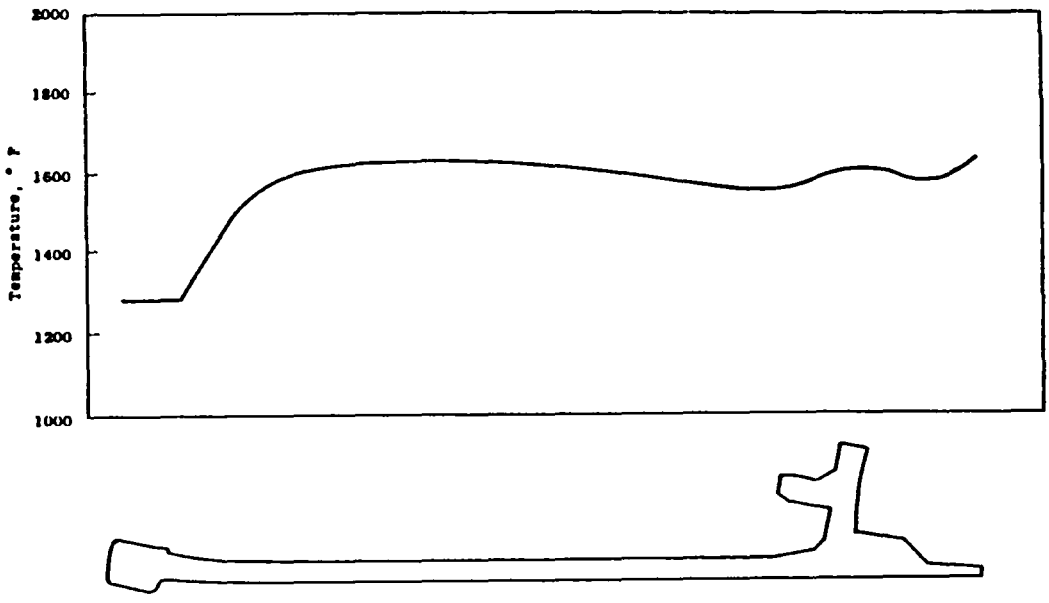

Figure 4. Axial Temperature Distribution W/O Hot Spot.

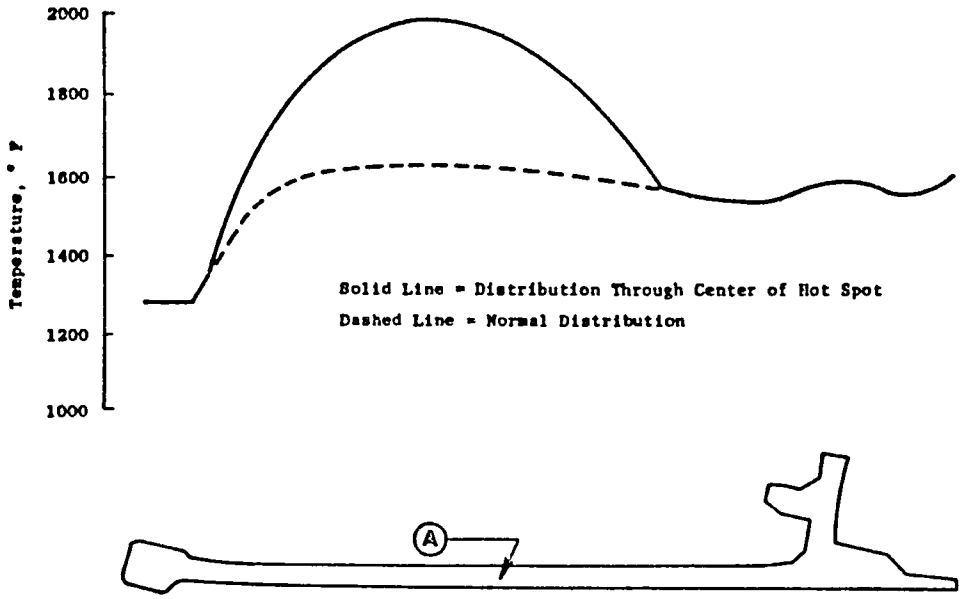

Figure 5. Axial Temperature Distribution Through Hot Spot.

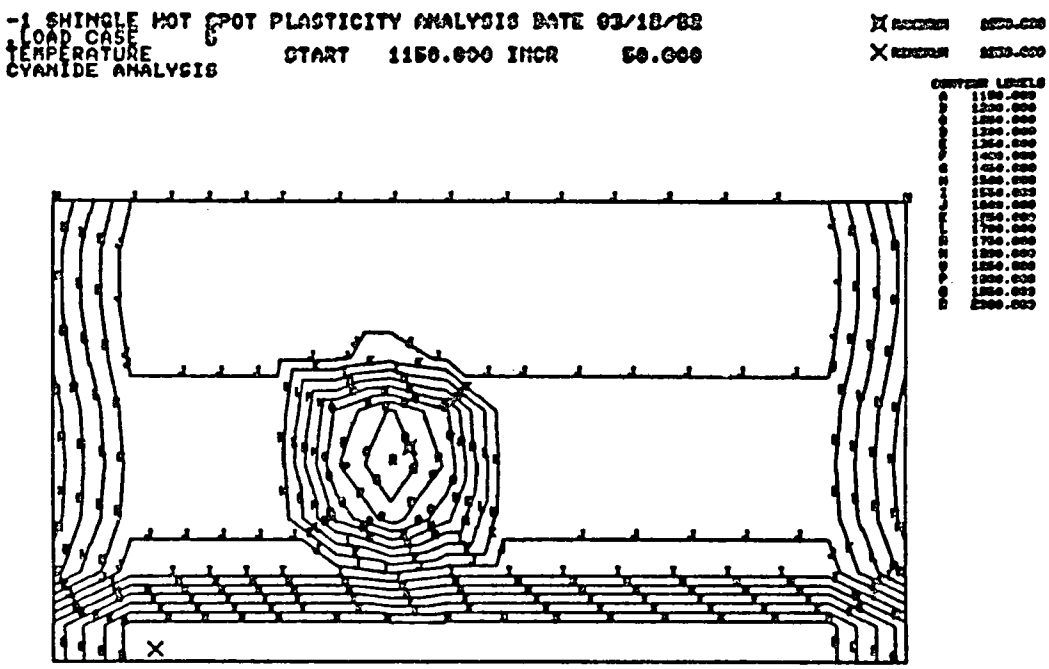

Figure 6. Temperature Contours At Peak Of Hot Spot

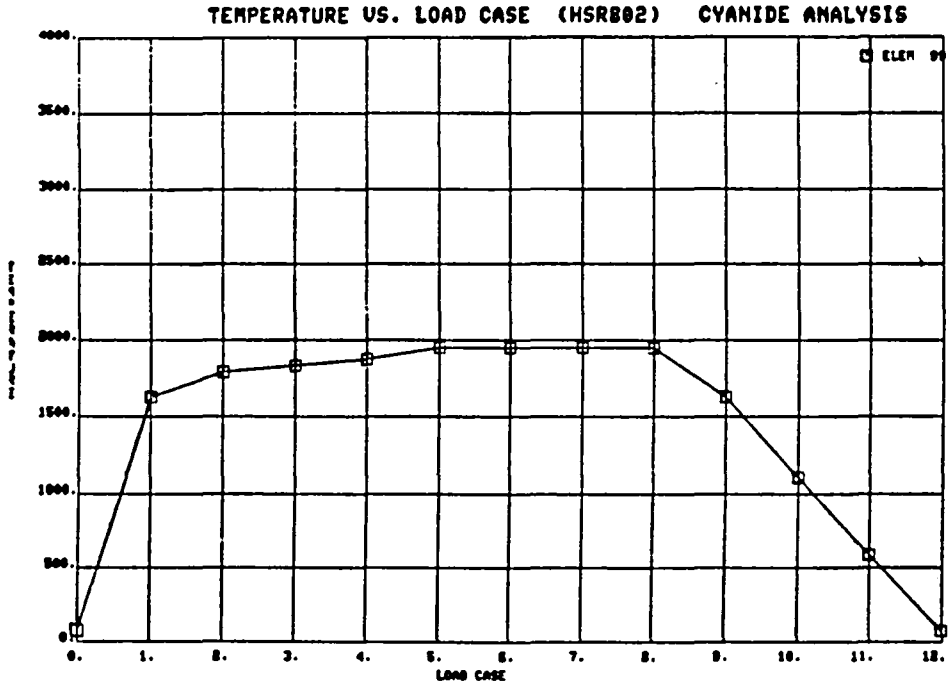

Figure 7. Heat-Up Cool-Down Cycle For Center Of Hot Spot

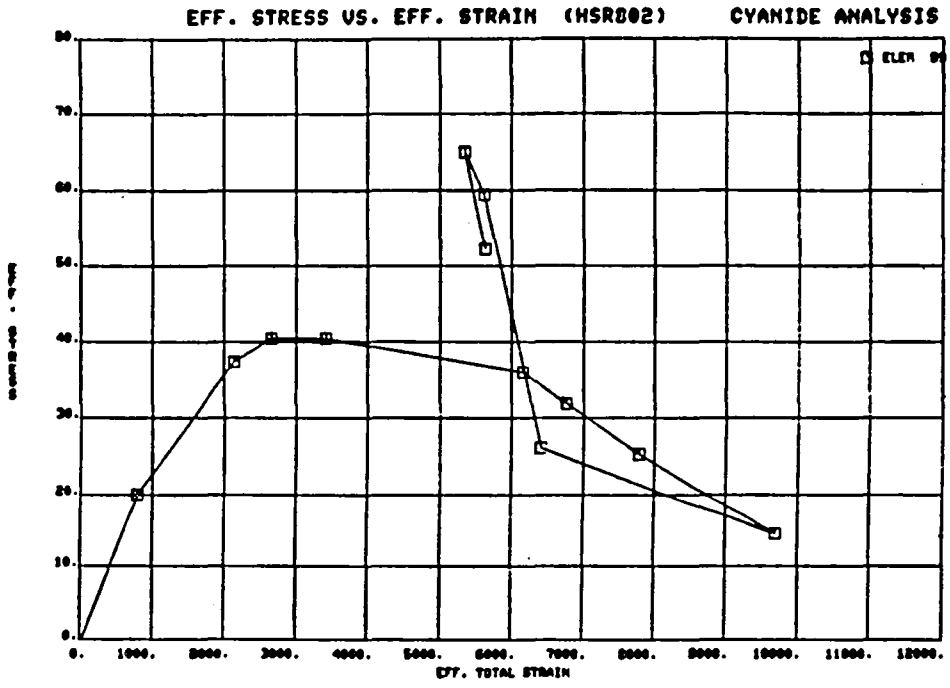

Figure 8. Effective Stress Versus Effective Strain At The Center of the Hot Spot For the First Cycle

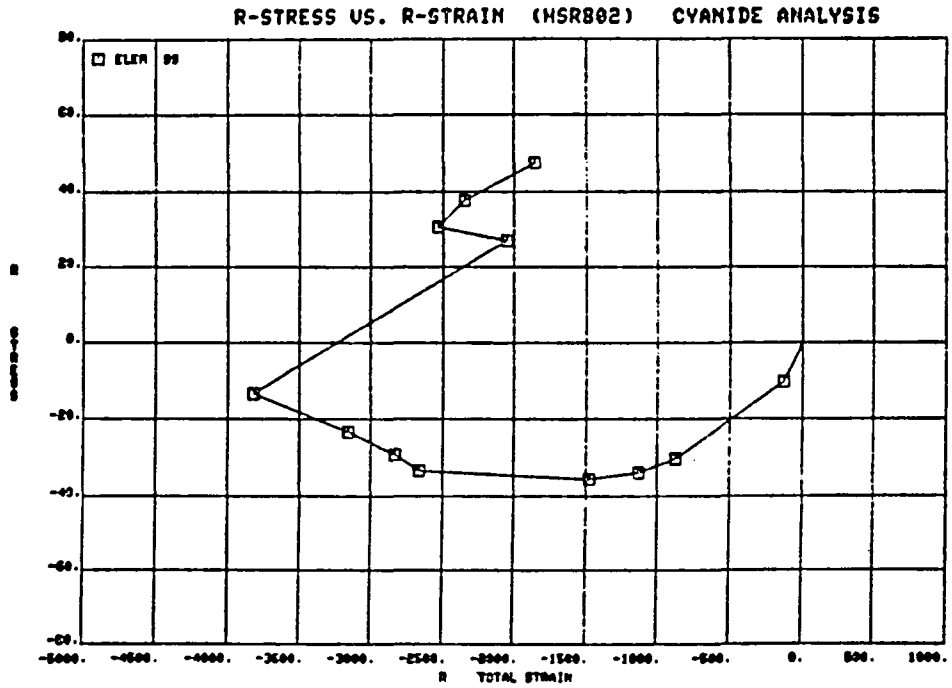

Figure 9. Transverse Stress Versus Strain At The Center of the Hot Spot For the First Cycle

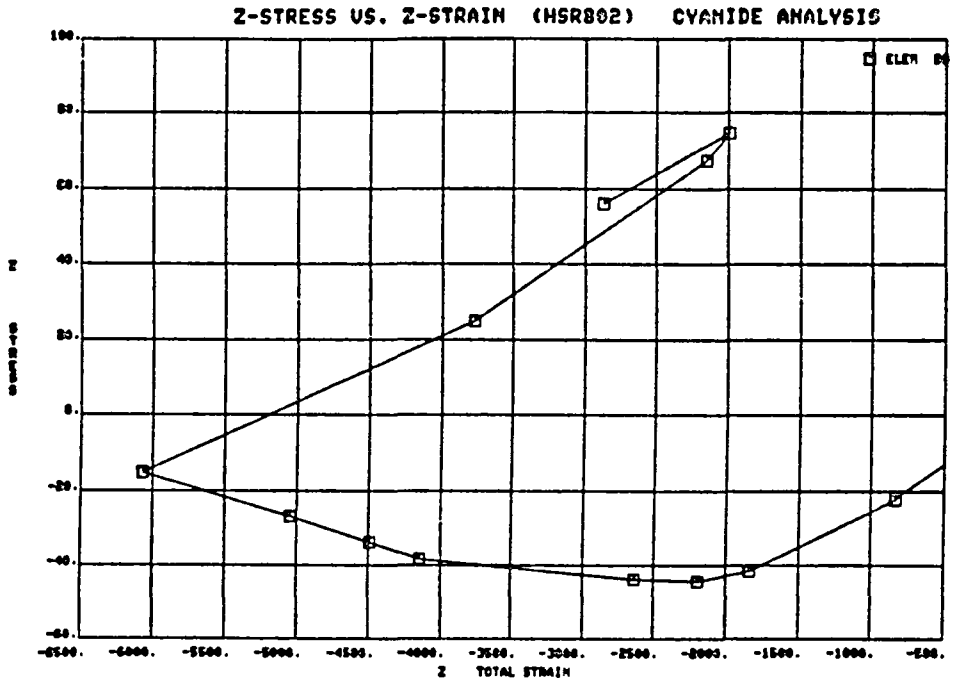

Figure 10. Longitudinal Stress Versus Strain At the Center of The Hot Spot For the First Cycle

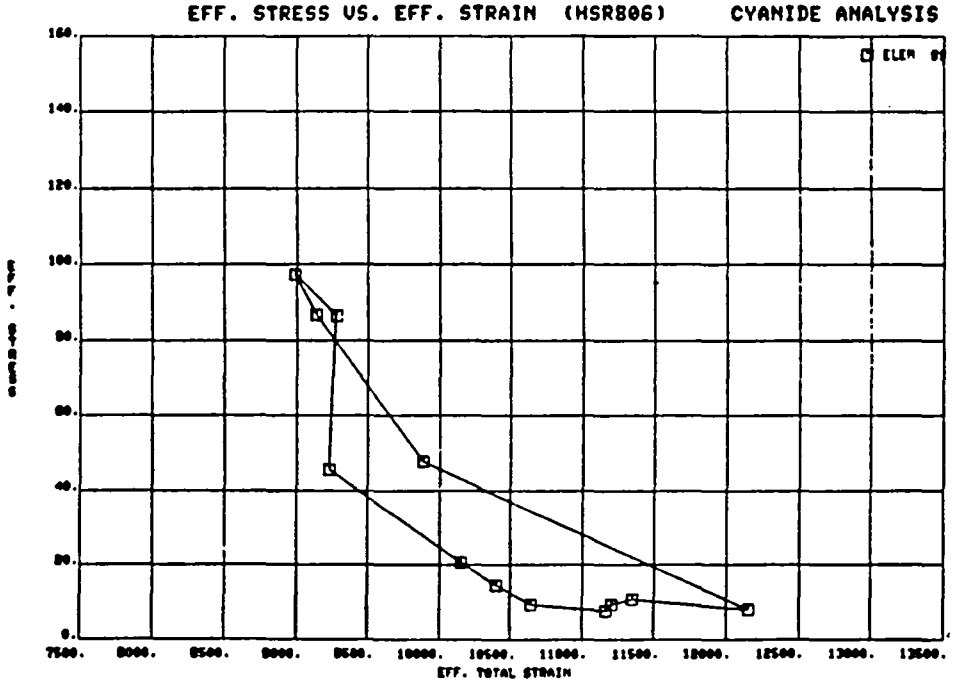

Figure 11. Shakedown Cycle of Effective Stress Versus Effective Strain At the Center of the Hot Spot

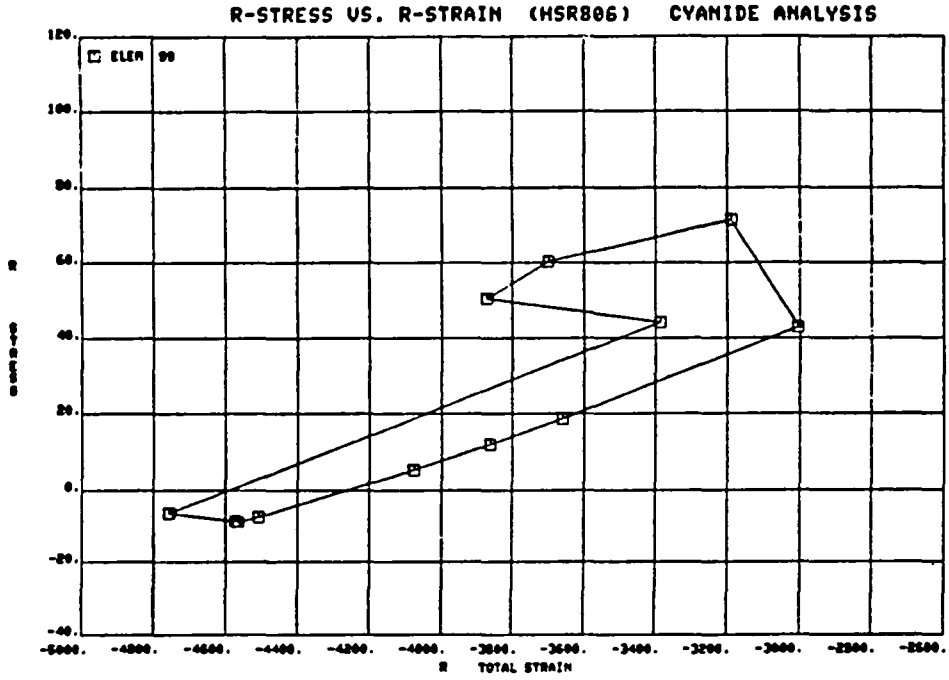

Figure 12. Shakedown Cycle For Transverse Stress Versus Strain At the Center of the Hot Spot

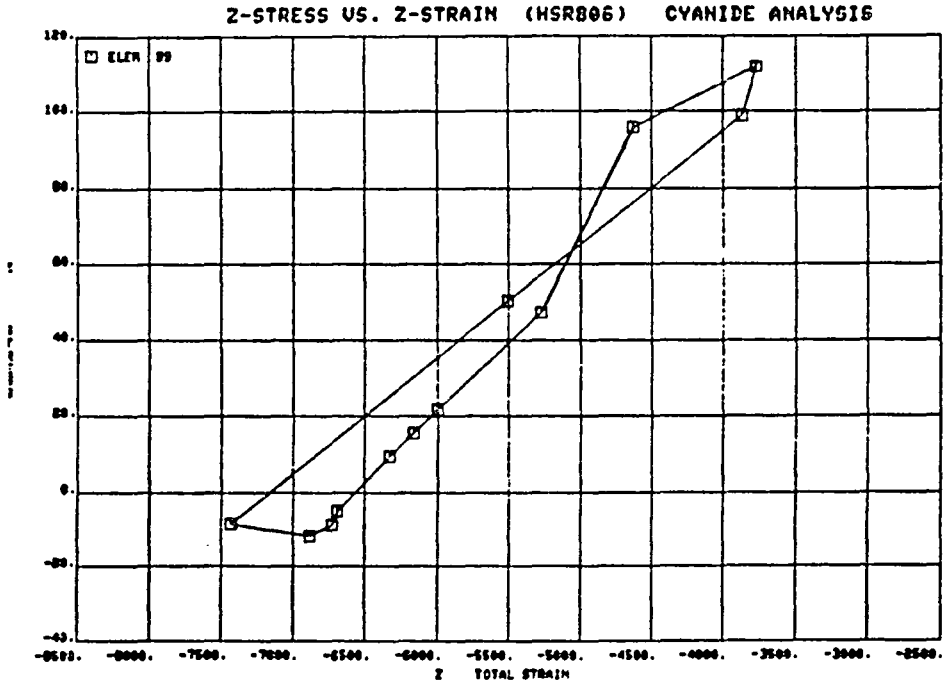

Figure 13. Shakedown Cycle For Longitudinal Stress Versus Strain at the Center of the Hot Spot

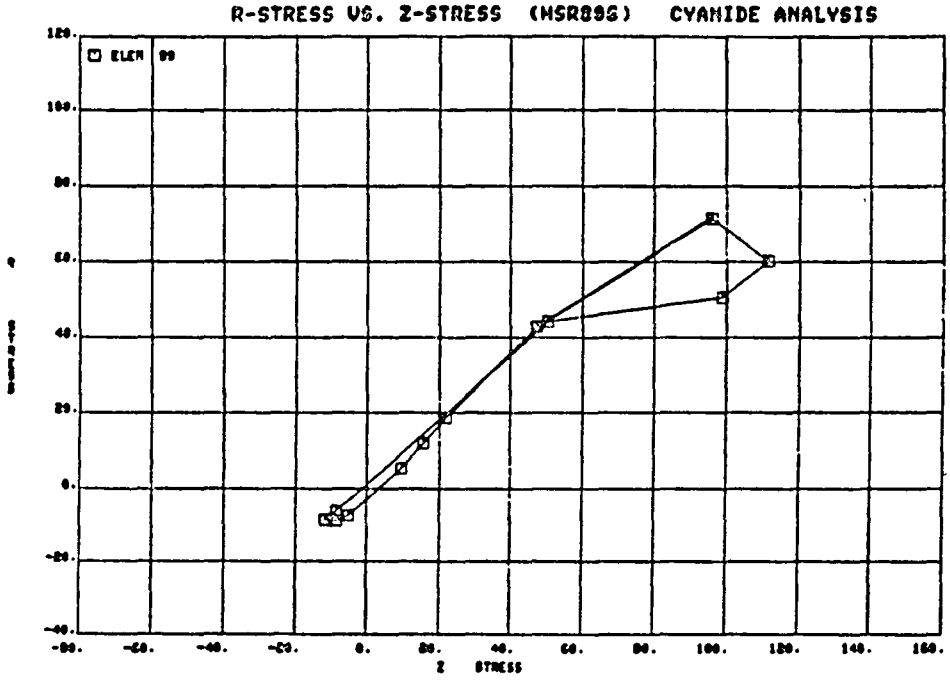

Figure 14. Shakedown Biaxial Stress Cycle At the Center Of the Hot Spot